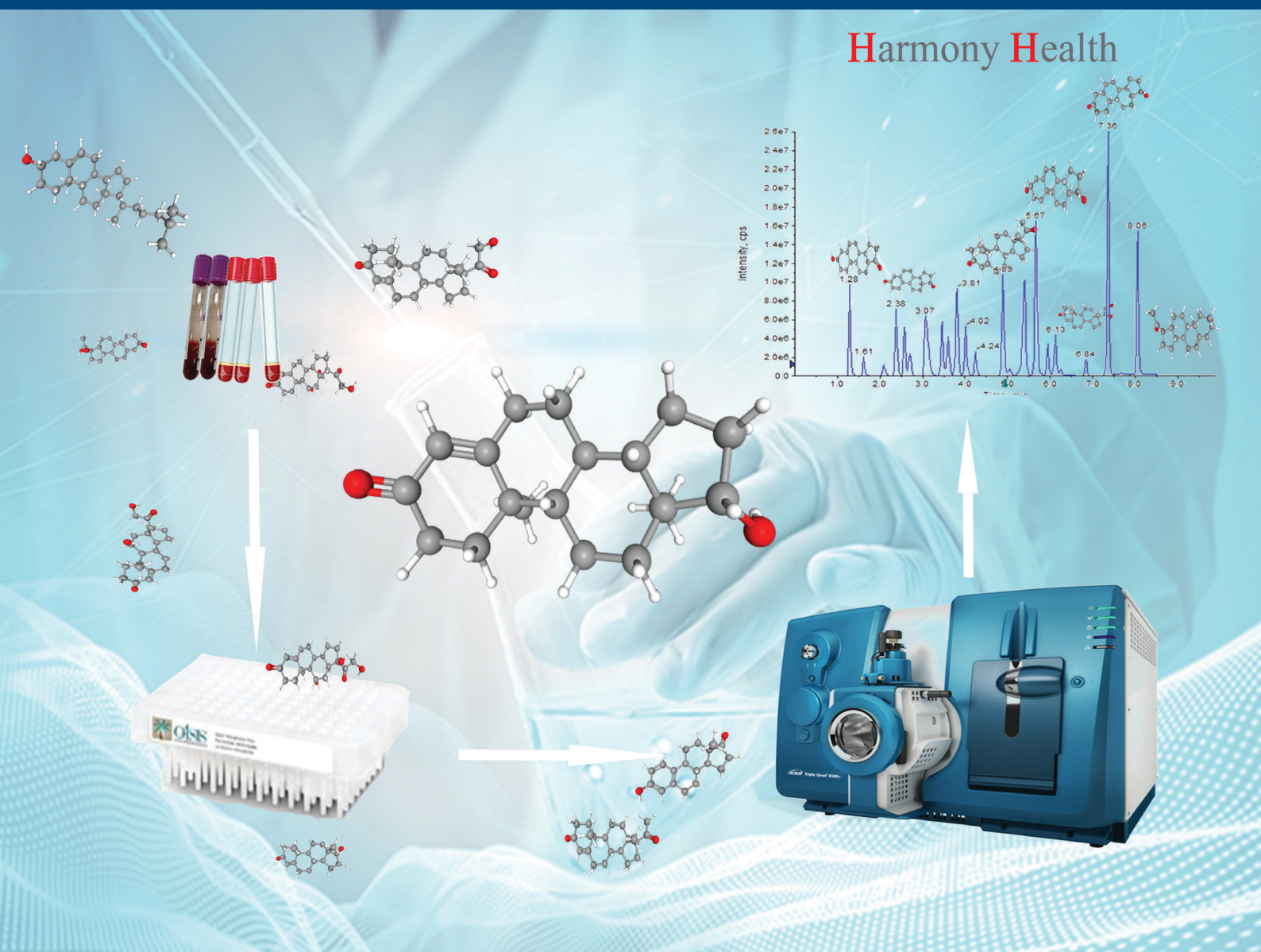
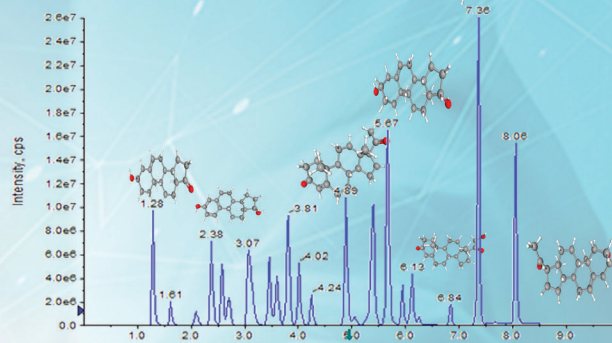


# JOURNAL OF SEPARATION SCIENCE

12 | 2021



Harmony Health



## Methods

Chromatography · Electroseparation

## Applications

Biomedicine · Foods · Environment

[www.jss-journal.com](http://www.jss-journal.com)

WILEY-VCH

## RESEARCH ARTICLE

# Determination of highly polar compounds in atmospheric aerosol particles at ultra-trace levels using ion chromatography Orbitrap mass spectrometry

Carlo Kwiezinski<sup>1</sup> | Christian Weller<sup>2</sup> | Dominik van Pinxteren<sup>1</sup> |  
Martin Brüggemann<sup>1</sup>  | Stephan Mertes<sup>3</sup> | Frank Stratmann<sup>3</sup> |  
Hartmut Herrmann<sup>1</sup> 

<sup>1</sup> Atmospheric Chemistry Department (ACD), Leibniz Institute for Tropospheric Research (TROPOS), Leipzig, Germany

<sup>2</sup> Thermo Fisher Scientific GmbH, Dreieich, Germany

<sup>3</sup> Experimental Aerosol and Cloud Microphysics Department, Leibniz Institute for Tropospheric Research (TROPOS), Leipzig, Germany

## Correspondence

Prof. Dr. Hartmut Herrmann, Leibniz Institute for Tropospheric Research (TROPOS), Atmospheric Chemistry Department (ACD), Permoserstr. 15, 04318 Leipzig, Germany.  
Email: [herrmann@tropos.de](mailto:herrmann@tropos.de)

A method using ion chromatography coupled to high-resolution Orbitrap mass spectrometry was developed to quantify highly-polar organic compounds in aqueous filter extracts of atmospheric particles. In total, 43 compounds, including short-chain carboxylic acids, terpene-derived acids, organosulfates, and inorganic anions were separated within 33 min by a KOH gradient. Ionization by electrospray was maximized by adding 100  $\mu\text{L min}^{-1}$  isopropanol as post-column solvent and optimizing the ion source settings. Detection limits ( $S/N \geq 3$ ) were in the range of 0.075–25  $\mu\text{g L}^{-1}$  and better than previously reported for 22 compounds. Recoveries of extraction typically range from 85 to 117%. The developed method was applied to three ambient samples, including two arctic flight samples, and one sample from Melpitz, a continental background research site. A total of 32 different compounds were identified for all samples. From the arctic flight samples, organic tracers could be quantified for the first time with concentrations ranging from 0.1 to 17.8  $\text{ng m}^{-3}$ . Due to the minimal sample preparation, the beneficial figures of merit, and the broad range of accessible compounds, including very polar ones, the new method offers advantages over existing ones and enables a detailed analysis of organic marker compounds in atmospheric aerosol particles.

## KEYWORDS

atmospheric aerosol, ion chromatography, method development, Orbitrap mass spectrometry, polar compounds

**Article Related Abbreviations:** A.U, arbitrary unit; AA, acetic acid; ACloud, Arctic CLOUD Observations Using airborne measurements during polar Day; careneOS, 2-hydroxy-carene organosulfate; CSA, camphorsulphonate; DCA, dicarboxylic acid; DTAA, diaterpenylic acid acetate; FA, formic acid; HAS, hydroxyacetone sulfate; HERA, High-Volume Aerosol Sampler; IC-CD, Ion chromatography-conductivity detection; IC-MS, Ion chromatography-mass spectrometry; IEC-MS, Ion exchange chromatography-mass spectrometry; IPC-UV, Ion-pair chromatography-ultraviolet spectroscopy detection; limonaketoneOS, limonaketone organosulfate; MBTCA, 3-methyl-1,2,3-butanetricarboxylic acid; MCA, monocarboxylic acid; MSA, methansulfonate; PAMARCMiP 2018, Polar Airborne Measurements and Arctic Regional Climate Model Simulation Project 2018.;  $\alpha$ -pineneOS, 2-hydroxy- $\alpha$ -pinene organosulfate

This is an open access article under the terms of the [Creative Commons Attribution-NonCommercial](https://creativecommons.org/licenses/by-nc/4.0/) License, which permits use, distribution and reproduction in any medium, provided the original work is properly cited and is not used for commercial purposes.

© 2021 The Authors. *Journal of Separation Science* published by Wiley-VCH GmbH

## 1 | INTRODUCTION

Aerosol particles in the atmosphere consist of inorganic substances and a large number of organic compounds. In contrast to the well-characterized inorganic fraction, much less is known about concentrations and sources of organic constituents. A significant fraction of the organic aerosol consists of small polar compounds, including low molecular weight mono- and dicarboxylic acids (MCAs and DCAs, respectively), terpene-derived acids, and organosulfates [1, 2]. These compounds originate from a variety of primary and secondary sources and are important tracers for the source assignment of aerosol particles. Small MCAs are emitted by the combustion of fossil fuels and biomass [3], or in a biogenic way by fungi, bacteria, pollen, and algae [4]. Small DCAs originate from cigarette smoke, the pyrolysis of vegetation, or fossil fuel combustion [5,6]. In general, organic acids are mainly formed secondarily from precursor gases. Plant-emitted isoprene is an important precursor for pyruvic acid, glyoxylic acid and glycolic acid [7], which can be subsequently oxidized to form oxalic acid [8,9]. In particular, pinonic, pinic, and norpinonic acid are a result of the photochemical oxidation of terpenes emitted by vegetation [10]. Similar to carboxylic acids, organosulfates are ubiquitously present in aerosol particles [2]. They can be formed by the reaction of organic precursor compounds with gaseous  $\text{SO}_2$  [11] or by acid-catalyzed multiphase reactions with acid sulfate aerosol [12–15]. Due to the lack of authentic standards, there are still uncertainties regarding concentrations in the ambient aerosol and the presence of unknown or unidentified organosulfates. Compared to ground measurements, relatively little is known about the composition of aerosol particles from high altitudes, as flights are expensive and measurements are difficult to perform. For polar latitudes and particularly the arctic region, only few flights have been performed until today, mostly focusing on inorganic tracers such as  $\text{SO}_4^{2-}$ ,  $\text{NO}_3^-$ , and metals [16–18]. The significance of organic components in this environment is still largely unclear. To enable the determination and quantification of organic tracers following in-flight sampling especially for high altitudes and polar latitudes, a highly sensitive method is needed that allows simultaneous determination of a large number of compounds with low sample consumption. So far in atmospheric aerosol samples, organic markers are determined with GC/MS [19], LC/MS [20], Ion chromatography-conductivity detection (IC-CD) [21] and CE [22]. GC/MS [23, 24] is characterized by high sensitivity and efficient analyte separation. For its application, carboxylic acids need to be derivatized to volatile compounds. They are usually concentrated by volume reduction in a vacuum, which makes sample preparation time-consuming and

potentially an error-prone working step [25]. IC-CD allows a simple, reliable, and inexpensive separation and quantification of water-soluble organic acids. The analysis is limited to ionic or ionizable and hydrophilic species and may suffer from peak overlap of individual compounds [21, 26] when a large number of species is present in the sample. Alternatively, CE is used for small carboxylic acids due to its fast separation and good separation efficiency [27]. The detection is mostly carried out by UV [28, 29], or via ESI coupled to MS [25, 27, 30]. Organosulfate analysis is performed by reversed-phase LC [12, 31] or hydrophilic interaction liquid chromatography (HILIC) coupled to MS [32, 33]. However, it is often challenging to separate these small polar compounds using reversed-phase LC [34], whereby HILIC separations are associated with reproducibility issues [35, 36]. Coupling advanced ion chromatography separation techniques to an Orbitrap mass spectrometer (IC-MS) is a promising alternative to overcome these separation issues and would allow for determining organic acids and organosulfates with a single method. In addition, the sample preparation could be uniformed to save time and sample volume. At the same time, MS detection allows a highly sensitive identification and quantification of low concentrated tracers from complex substance mixtures. Up until today, IC-MS has been used for surface-water [37], food samples [38], forensics samples [39], urine samples [40], and pesticides [41]. In the field of atmospheric science, only a few IC-MS applications are known, focusing on inorganic anions and carboxylic acids [42, 43]. The objective of the present study was the development of an IC-MS method, enabling the separation and sensitive detection of a large number of anionic compounds in aqueous aerosol particle extracts from arctic flight and continental ground measurements. Therefore, IC was coupled with an Orbitrap-MS and a standard mixture containing inorganic ions, organosulfates, mono-, di-, and tricarboxylic acids, and terpene-derived acids was used for method development. In order to optimize the LODs, various organic post-column solvents as well as basic and acidic additives and ESI source parameters were varied and tested. The final method was validated and used to quantify the analytes in aqueous extracts of aerosol particles from different sites.

## 2 | MATERIALS AND METHODS

### 2.1 | Chemicals

Standard compounds were obtained from Sigma Aldrich (St. Louis, USA), and Santa Cruz Biotechnology

(Huston, USA) in purity >95% or synthesized (Supporting Information Table S1). Stock solutions of all analytes were prepared by dissolution in ultrapure water (>18.20 M $\Omega$ /cm). From the stock solutions, a standard mixture was prepared, which included the MCAs glyoxylic acid, glycolic acid, pyruvic acid, the homologous series of DCAs from oxalic acid up to azelaic acid, the substituted DCAs methylsuccinic, methylmalonic, dimethylmalonic, fumaric, mesaconic, maleic, malic, citraconic, tartaric and tartronic acid, as well as the tricarboxylic acid citric acid. In addition, the terpene-derived acids pinic acid, cis-pinonic acid, 3-methyl-1,2,3-butanetricarboxylic acid (MBTCA), diaterpenylic acid acetate (DTAA), norpinonic acid, trans-norpinic acid, terebic acid, camphoric acid, a series of organosulfonates and -sulfates including hydroxyacetone sulfate (HAS), limonaketone organosulfate (limonaketoneOS), 2-hydroxy- $\alpha$ -pinene organosulfate ( $\alpha$ -pineneOS), 2-hydroxy-carene organosulfate (careneOS), mannose-6-sulfate, methylsulfate, methansulfonate (MSA), the organosulfate surrogates camphorsulphonate (CSA), and octylsulfate, and the inorganic ions sulfate, sulfite and bromide were included. To stabilize sulfite, a small volume of formaldehyde solution (37 %, Merck, Darmstadt, Germany) was added as an oxidation inhibitor. The KOH eluent cartridge for the IC was purchased from Thermo Fisher Scientific, Waltham, USA. Organic post-column solvents acetonitrile (ACN) and methanol (MeOH) were obtained in LC-MS grade from Fisher Scientific (Loughborough, UK). LC-MS Chromasolv™ isopropanol (IPA) was purchased from Honeywell. LiChropur® ammonium hydroxide solution (25 %), LiChropur® formic acid (puriss.  $\geq$  98 %), and LiChropur® acetic acid (puriss.  $\geq$  98%) were purchased from Merck as acidic and basic additives.

## 2.2 | Setup of the ion chromatography Orbitrap MS system and used software

For separation, a Dionex Integrion High Pressure Ion Chromatography (Thermo Fisher Scientific, Waltham, USA) system consisting of a pump, an eluent generator, a continuously regenerated anion trap column, an autosampler, a suppressor, and a conductivity detector was used. After separation, a defined flow of an organic post-column solvent was added via T-piece into the aqueous eluent stream through an external Vanquish pump (Thermo Fisher Scientific, Waltham, USA). The flow was then led into the ESI source of a Q Exactive Plus mass spectrometer (Thermo Fisher Scientific, Waltham, USA). For instrument control and data recording, Chromeleon 7.2 and the Xcalibur software bundle (4.0.27.19) were used.

## 2.3 | Separation and ionization conditions

For separation, the AS19-4  $\mu$ m separation- and an AG19-4  $\mu$ m guard column, were used at 30°C. A volume of 5  $\mu$ L was injected in partial loop mode. The method runtime was 42 min utilizing a multi-step KOH gradient. The initial KOH concentration was set to 10 mM, held for 6 min, and increased linearly with different slopes to 45 mM, 60 mM, and 100 mM after 21, 23, and 25 min, respectively. After reaching the maximum KOH-concentration, the mobile phase composition was held for 6 min and then set back to 10 mM for 11 min of equilibration. The eluent flow rate was set to 0.25 mL min<sup>-1</sup>, while a flow of 0.10 mL min<sup>-1</sup> IPA was added post-column. The solvent mixture, including the analytes, was led into the ESI source and ionized according to the following parameter settings: capillary temperature of 253°C, spray voltage of 3.25 kV, aux gas flow rate of 5 arbitrary unit (A.U.), sheath gas flow rate of 46 A.U., and the aux gas heater temperature of 406°C. The probe was set to position D while the Orbitrap was operated in full-MS-negative mode with a resolution of 35 000 in the range of 50–300 *m/z*.

## 2.4 | Optimization and validation of the ion chromatography Orbitrap MS coupling

To improve the signal intensity of the method and thus its LOD, the influence of the flow rate of organic post-column solvents, the volume fraction of acidic and basic additives, and the ESI source parameters were investigated in the order mentioned above. For this purpose, a standard mixture containing all compounds at a concentration of 50  $\mu$ g L<sup>-1</sup> was used, and the influence of each investigated parameter on the cumulative peak area was determined. After each optimization step, the largest cumulative peak area was selected as starting point for further investigations. For method validation, the final optimized IC-MS method LODs (*S/N*  $\geq$  3) were determined by analyzing dilution series of standard mixtures. If an *m/z* trace showed no noise, the lowest detectable concentration was set as the LOD. The calibration function was determined from a series of 15 standard mixtures ranging from 0.025 to 500  $\mu$ g L<sup>-1</sup>. The RSD of peak area (PA) was used to characterize interday- and intraday repeatability. Intraday repeatability was determined by nine and interday repeatability by three injections of the same standard mixture on the same and on three different days, respectively. The recoveries of aqueous sample extraction were determined from spiked filters, as appropriate reference materials for these analytes in ambient particles are not available. Therefore, 47 mm polycarbonate filter

(Whatman, Little Chalfont, UK) and 13 mm quartz fiber filter (MK 360, 180 Munktell, Sweden) were spiked with a defined volume of a 1000  $\mu\text{g L}^{-1}$  standard solution. The filters were dried and transferred to a pre-cleaned 5 mL syringe (Omnifix, Braun, Melsungen, Germany). To simulate the different extraction protocols applied for real samples, either 3 mL or 0.25 mL of ultrapure water was added to a 47 mm polycarbonate filter, while 0.25 mL was added to a quartz fiber filter. Afterwards, the solutions were shaken for 2 h at 420 rpm. The resulting extracts were filtered through a 0.2  $\mu\text{m}$  syringe filter (Acrodisc 13, Pall, Dreieich, Germany), transferred into a vial, and measured with the developed method. Mean recoveries were determined from five replicate experiments. In parallel, three non-spiked filters were used as a reference.

## 2.5 | Sampling and sample extraction

For testing the method, three ambient samples were analyzed (I) from a flight of the ACLOUD campaign (Arctic CLOUD Observations Using airborne measurements during polar Day) [44], (II) from the rural background station Melpitz in Germany (12° 56' E, 51° 32' N) and (III) from a flight of the PAMARCMiP 2018 (Polar Airborne Measurements and Arctic Regional Climate Model Simulation Project 2018). During ACLOUD, the research aircraft POLAR 6 started on June 8th and 9th 2017 from Longyearbyen, Svalbard (15° 38' E, 78° 13' N) and flew over the arctic ocean towards the pack ice above 80° N and back. By means of a Counterflow Virtual Impactor Inlet [45] which was operated to sample ambient aerosol particles, 1.12 m<sup>3</sup> ambient air was accumulated on a 13 mm fiber filter (MK 360, Munktell, Sweden). Furthermore, a sample was taken with the in-house developed High-Volume Aerosol Sampler (HERA) on 26<sup>th</sup> January 2018 at the Melpitz research station in Germany. The HERA sampler was operated in a measurement container and connected via stainless steel tubing to an existing inlet. With a pump, atmospheric particulate matter with an upper aerodynamic diameter of 10  $\mu\text{m}$  (PM<sub>10</sub>) was accumulated with a flow rate of 0.0167 m<sup>3</sup> min<sup>-1</sup> for 24 h on a 47 mm polycarbonate filter (Whatman, Little Chalfont, UK). After first tests at the ground station of Melpitz, the prototype of HERA was also used during the PAMARCMiP 2018 campaign at the research aircraft Polar 5. On 2nd April 2018, the aircraft took off from Villum research station in Greenland (81° 36' N, 16° 40' W) into direction of Svalbard. Halfway along the route, the aircraft turned back and made targeted flights over the Arctic Ocean and along the pack ice border. During the flight, the HERA sampler was connected over a ~6 m long, horizontal stainless-steel tube with a shrouded inlet diffuser mounted at the outside of the aircraft [46]. Thus, aerosol particles of 2.32 m<sup>3</sup>

ambient air were accumulated on a 47 mm polycarbonate filter. After sampling, all filters were stored at a temperature < 0°C. For extraction, the ACLOUD filter was shaken in 0.25 mL ultrapure water at 420 rpm for 2 hours. The filters of the Melpitz- and PAMARCMiP-campaign were part of an interdisciplinary analysis protocol, in which in addition to their chemical composition other sample properties were investigated. Therefore, their extraction protocol differed as follows: The filters were shaken in 3 mL ultrapure water and 2.9 mL of the resulting extract was diluted with 3.1 mL ultrapure water. To protect the column from remaining particles, all extracts were filtered with a pre-cleaned 5 mL syringe (Omnifix, Braun, Melsungen, Germany) through a 0.2  $\mu\text{m}$  syringe filter (Acrodisc 13, Pall, Dreieich, Germany), transferred into the vial, and measured with the developed IC-MS-method.

## 3 | RESULTS AND DISCUSSION

### 3.1 | Method optimization

#### 3.1.1 | Separation conditions

Even with an MS detector, the choice of the IC-column has to be made carefully in order to elute as many compounds as possible with good separation, peak shapes, and S/N. Although anion exchange is the dominating separation mechanism, the hydrophobicity of the column stationary phase also affects the retention of the analytes. The Virtual Column Separation software implemented in Chromeleon 7.2 uses a data set of known retention times of compounds to suggest appropriate columns. For bromide, nitrate, sulfite, sulfate, glycolate, pyruvate, malonate, maleate, glutarate, malate, tartrate, oxalate, fumarate, and citrate, the software proposed to use the AS11-HC-4  $\mu\text{m}$  or AS19-4  $\mu\text{m}$  separation column. Due to its medium-low hydrophobicity, the AS11-HC-4  $\mu\text{m}$  typically is the column of choice for the separation of small polar organic acids, but is unsuitable for the separation of larger organosulfates. Therefore, the AS19-4  $\mu\text{m}$  column with low hydrophobicity was chosen for further investigations. For separation, the standard flow rate of 0.25 mL min<sup>-1</sup>, the column temperature of 30°C and the KOH gradient were adopted from the AS19-4  $\mu\text{m}$  column manual. Then a last 100 mM step was added to the KOH gradient to elute highly retained species and free the column from possible matrices of the sample extracts. Figure 1 shows the chromatogram for a 50  $\mu\text{g L}^{-1}$  standard, where all compounds are separated within 33 min. Shorter polar MCAs in the form of glycolate, pyruvate, and glyoxylate, as well as the organosulfonate MSA and the monoterpene-derived norpinonate, terebate, and

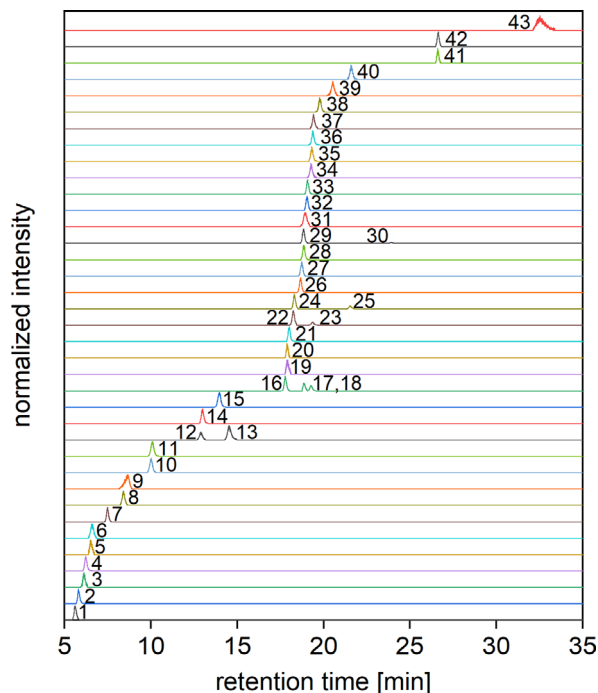


**FIGURE 1** Chromatogram of the multi-standard (concentration  $50 \mu\text{g L}^{-1}$ ) using an ASI9-4  $\mu\text{m}$  column. (1) Glycolate, (2) Norpinonate, (3) Terebate, (4) cis-Pinonate, (5) Pyruvate, (6) MSA, (7) Glyoxylate, (8) CSA, (9) LimonaketonOS, (10) Methylsulfate, (11) HAS, (12)  $\alpha$ -PineneOS, (13) CareneOS, (14) Bromide, (15) Nitrate, (16) Dimethylmalonate, (17) Glutarate, (18) Methylsuccinate, (19) Mannose-6-sulfate, (20) Sulfate, (21) Sulfite, (22) Methylmalonate, (23) Succinate, (24) Citraconate, (25) Mesaconate, (26) Malonate (27) DTAA, (28) Malate, (29) Maleate, (30) Fumarate, (31) trans-Norpinate, (32) L-Tartrate, (33) Tartronate, (34) Pinate, (35) CA, (36) Adipate, (37) Oxalate, (38) Pimelate, (39) Suberate, (40) Azelate, (41) Citrate, (42) MBTCA, (43) Octylsulfate

cis-pinonate elute earliest between 5.62 and 7.51 min. All inorganic ions and organosulfates, except octylsulfate, can be detected between 8.39 and 18.03 min. The dicarboxylic, the tricarboxylic and the remaining terpene-derived acids elute in a time window of 17.78–26.66 min. Octylsulfate elutes last from the column after 32.52 min. Coelution is observed for (I) methylsulfate and hydroxyacetonesulfate at 10.01 min, (II) dimethylmalonate, sulfate, and mannose-6-sulfate at 17.89 min, (III) methylmalonate and citraconate at 18.25 min, (IV) malonate and DTAA at approximately 18.68 min, (V) maleate, malate, and glutarate at 18.85 min, (VI) L-tartrate and tartronate at 19.04 min, (VII) methylsuccinate, pinnate, and camphorate at 19.27 min, (VIII) succinate, adipate, and oxalate at 19.40 min, and (IX) mesaconate and azelate at 21.53 min. However, all isomeric analytes are completely baseline separated. The organosulfates limonaketonOS, careneOS, and octylsulfate showed peak widths up to 0.7 min because of peak fronting and tailing. The remaining compounds elute in excellent peak shapes.

### 3.1.2 | Optimization of the post-column solvent

To enhance ESI and to optimize sensitivity, organic solvents comprising MeOH, ACN, and IPA were added post-column to the IC effluent. The influence of this post-column addition on single analyte peak areas, as well as their cumulative peak areas, was investigated. For each organic post-column solvent, the flow rate was varied in  $50 \mu\text{L min}^{-1}$  increments from 50 to  $450 \mu\text{L min}^{-1}$  (Figure 2). For MeOH and ACN (Figure 2A and B), the normalized peak areas of almost all analytes increase with higher flow rates of up to 250–350  $\mu\text{L min}^{-1}$  and 300–400  $\mu\text{L min}^{-1}$ , respectively. Above these ranges, signals mostly remain constant or start to decrease. For IPA (Figure 2C), a flow rate of up to 100  $\mu\text{L min}^{-1}$  led to a small increase in peak areas for the majority of analytes, whereas higher flow rates yielded lower signal intensities for most compounds instead. In general, ESI response was increased when adding organic solvents due to their low surface tensions, low dielectric constants [47], low boiling points [48], and high gas-phase proton affinities [49]. On the other hand, since ESI-MS is a concentration-sensitive technique [50], the addition of post-column solvents dilutes the IC effluent, leading to a decreasing cumulative peak area at higher flow rates [48]. Furthermore, excessive flow rates were previously shown to lower ionization efficiency due to the formation of larger droplets at the ESI emitter [51, 52]. From the cumulative peak areas in Figure 2D, it can be seen that on average for flow rates up to 300  $\mu\text{L min}^{-1}$ , the MS response is strongest for IPA among the three different solvents. At higher flow rates, MeOH exhibits slightly stronger signal intensities, whereas ACN always gives the weakest average response. A possible explanation could be the formation of a more stable spray when using MeOH and IPA compared to ACN. According to Straub and Voyksner [53], this is due to the higher onset voltage (the lowest voltage, at which electric discharge takes place) of both solvents, preventing the formation of an electrical discharge that can interfere with the spray formation. Since the use of a flow rate of 100  $\mu\text{L min}^{-1}$  IPA leads to the largest growth of the cumulative peak area, it is used as post-column solvent for further optimization steps.

### 3.1.3 | Influence of post-column solvent additives

To test for possible further increases of detection sensitivity, acidic and basic additives, i.e., formic acid (FA), acetic acid (AA), and ammonium hydroxide ( $\text{NH}_4\text{OH}$ ), were added to the post-column injection of IPA in volumetric proportions of 0.1–0.5 vol%. As can be seen from Figure 3,

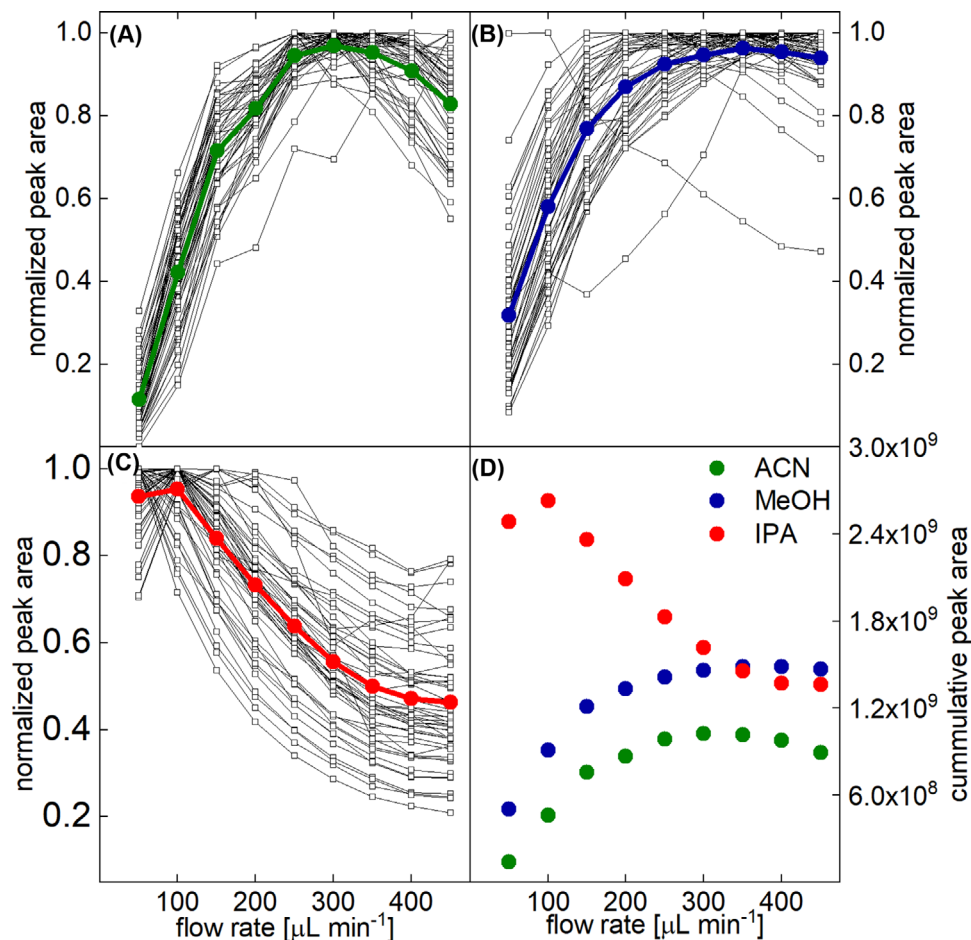


FIGURE 2 Dependence of the normalized peak area on the flow rate of added (A) ACN (green), (B) MeOH (blue), and (C) IPA (red). Black lines indicate individual analytes, and colored lines correspond to the mean values determined from all compounds. Panel (D) shows cumulative peak areas of all components

all additives led to a decrease in signal intensities, thus giving the highest cumulative peak areas for pure IPA. For  $\text{NH}_4\text{OH}$ , a continuous decrease in the cumulative peak area was observed with increasing additive fractions. For both acids, the determined cumulative peak areas remain at approximately the same level, which was lower for FA than for AA. Additional protons from the acids could lead to a neutralization of the analyte ions and thus to a decrease of the cumulative peak areas. Considering the lower  $\text{p}K_a$  value of FA (3.75) compared to AA ( $\text{p}K_a$  4.75), more protons are formed when using FA, explaining the lower cumulative peak area. Also, signals of formate dimers ( $m/z = 91.00$ ) and acetate ( $m/z = 59.01$ ) were observed in the mass spectra and could cause suppression effects in the ESI [54] that decrease the signal intensity. Suppression effects could also explain the continuous decrease in signal intensity for the use of  $\text{NH}_4\text{OH}$ , since in the mass spectra the formation of intensive background signals at  $m/z$  57.03 and 60.01 are detectable. Overall, regardless of the nature and quantity of additive added, no increase in the cumulative peak area could be achieved.

Therefore, the optimization was continued with pure IPA at a flow rate of  $100 \mu\text{L min}^{-1}$ .

### 3.1.4 | Optimization of the ESI source parameters

In the last step, the ESI source parameters were optimized. Starting points were suggested by the Tune software (Thermo Fisher Scientific, Waltham, USA) for a flow rate of  $250 \mu\text{L min}^{-1}$  as follows: capillary temperature of  $253^\circ\text{C}$ , spray voltage of 2.5 kV, auxiliary gas flow rate of 11 A.U., sheath gas flow rate of 46 A.U., auxiliary gas heater temperature of  $406^\circ\text{C}$ . For the optimization, the parameters were systematically changed in the order mentioned above, keeping all other settings constant at the value leading to maximum cumulative peak areas. If no change in response could be observed, the initial value was used. As shown in Figure 4A, the capillary temperature did not lead to significant changes in the cumulative peak area, hence the suggested temperature of  $253^\circ\text{C}$  was used. In

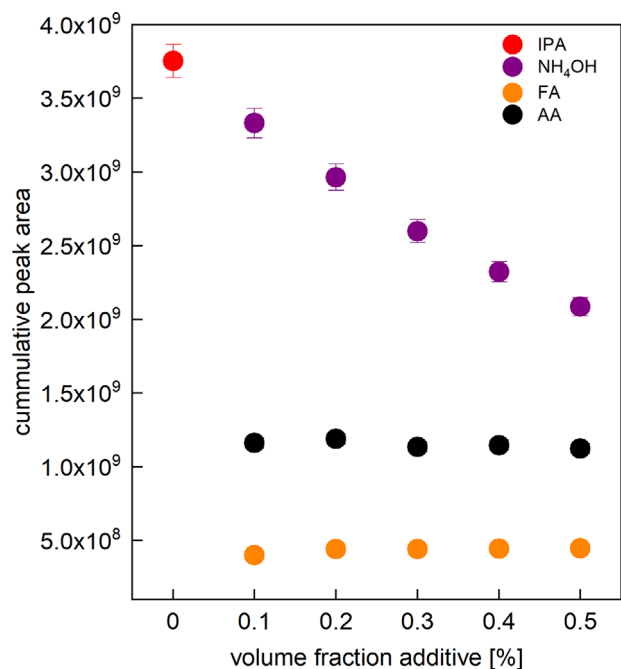


**FIGURE 3** Influence of the post-column solvent additive on the cumulative peak area from IPA (red) at a flow rate of  $100 \mu\text{L min}^{-1}$  and added portions of AA (black), FA (orange), or  $\text{NH}_4\text{OH}$  (blue)

contrast, the spray voltage had a strong influence on signal intensities giving a maximum at 3.25 kV (Figure 4B). The optimum spray voltages provide a stable Taylor cone at the tip of the ESI-needle, where ion-containing droplets of a certain size are formed [55]. At lower and higher voltages, unfavorable effects on the Taylor cone likely led to the observed lower signal intensities. The auxiliary gas flow rate, sheath gas flow rate, and auxiliary gas heater temperature assist the desolvation by adjusting the amount and temperature of introduced  $\text{N}_2$ -drying gas. In addition to this, the auxiliary gas flow rate and sheath gas flow rate focus the spray into the direction of the MS-entrance [56]. Best results were found for an auxiliary gas flow rate of 5 A.U. and a sheath gas flow rate of 46 A.U. The mean values of the cumulative peak areas of the aux gas heater temperatures of 356, 406, and  $456^\circ\text{C}$  were within the uncertainty range of the measurements, with a maximum of  $4.96 \times 10^9$  at  $406^\circ\text{C}$ , which was chosen for further measurements. As can be seen in Figure 4F, the spray voltage and the auxiliary gas flow rate have the greatest influence on the cumulative peak area. As mentioned above, the spray voltage determines the stability of the spray and the size of the ion-carrying droplets and thus significantly affects the number of formed ions [55]. Similarly, the auxiliary gas flow rate, sheath gas flow rate, and aux gas heater temperature influence the efficiency of the ESI process [56, 57], which explains the observed impact of

these parameters on signal intensities. Since the aux gas flow rate was optimized first, the corresponding influence is the greatest. For method validation, the following final ESI settings were used: capillary temperature of  $253^\circ\text{C}$ , spray voltage of 3.25 kV, auxiliary gas flow rate of 5 A.U., sheath gas flow rate of 46 A.U. and the auxiliary gas heater temperature of  $406^\circ\text{C}$ .

### 3.2 | Method validation

The optimized method was validated by analyzing a series of standard mixtures with 43 compounds. The resulting figures of merit and LODs from other methods are summarized in Table 1. For the 47 mm polycarbonate filters extracted with 0.25 mL ultrapure water, determined recoveries were in the range of 85–117% and are thus considered sufficiently close to a complete extraction of the analytes from the filter material. Similar results for the extraction of the polycarbonate filter with 3.00 mL and the extraction of the quartz fiber filter with 0.25 mL are listed in Table S2. With regards to the measured peak area, intraday and interday repeatability were below 3.0 % for all compounds except for nitrate, fumarate, and citrate. Both, linear and quadratic regression lines were applied in the calibration ranges from 0.25 to  $500 \mu\text{g L}^{-1}$ . To reduce the error of the calibration function a  $1/X$  or  $1/X^2$  weighting was applied. The obtained coefficients of determination  $R^2$  ranging from 0.9659 to 0.9996 and can be considered as satisfactory. The LODs of all analytes are between 0.075 and  $25 \mu\text{g L}^{-1}$  and are compared to most sensitive reported ones from the literature. For inorganic anions, best available LODs from the literature tend to show a factor of 11–3116 higher LODs, except for nitrate, where the LOD of the IC-MS method is a factor of 5 lower than the literature reference. In the case of MCAs, the LODs are equal or lower by up to a factor of 16. Among the 18 di- and tri-carboxylic acids, the LODs of oxalate, glutarate, dimethylmalonate, methylsuccinate and L-tartrate could be improved by a factor of up to 130. The LODs of methylmalonate, citraconate, malonate, malate and adipate were about a factor of 2 lower or higher. Reference studies with lower LODs could be found for succinate, pimelate, suberate, azelate, fumarate, maleate, and citrate. For the remaining DCAs, no corresponding literature reference could be found. The same applies to the terpene-derived compounds DTAA, terebate, trans-norpinate, and camphorate, except for pinate with LODs of the developed IC-MS method being nearly equal or greater by a factor of 10 than the best available literature LOD. Among the organosulfates, similar to the literature references LODs could be found for all compounds except the surrogate mannose-6-sulfate. For HAS and methylsulfate, the LODs of the IC-MS are lower by a factor of 35. For



TABLE 1 Figures of merit for the optimized IC-MS-method and LOD comparison with best reported values from other methods

Compound	Signal [M-H] <sup>-</sup> m/z	Repeatability		Recovery Polycarbonate filter 0.25 mL extraction %	Calibration		R <sup>2</sup>	Weighting function	Limit of detection		Method and reference for LOD comparison		
		Intraday (RSD) %	Interday (RSD) %		Calibration range µg L <sup>-1</sup>	Calibration function			LOD IC-MS µg L <sup>-1</sup>	LOD ref- erences µg L <sup>-1</sup>			
<b>Inorganic anions</b>													
Bromide	78.919	13.00	1.38	0.16	101	0.25-500	linear	1/X	0.9961	1/X	0.1	49	IC-CD [58]
Nitrate	61.988	13.97	4.87	4.38	117	50-500	linear	Equal	0.9988	Equal	25	5	IC-CD [59]
Sulfate	96.960	17.89	2.30	2.25	861	50-500	linear	Equal	0.9877	Equal	10	109	IC-CD [58]
Sulfite	80.965	18.03	0.67	0.19	90	2.5-500	square	1/X	0.9971	1/X	0.5	1558	IPC-UV [60]
<b>Monocarboxylic acids</b>													
Glycolate	75.009	5.62	1.49	0.71	109	10-500	linear	1/X	0.9969	1/X	2.5	40	CE-UV [61]
Pyruvate	87.009	6.50	2.48	2.67	86	25-500	linear	1/X	0.9923	1/X	5	5	LC-MS [62]
Glyoxylate	72.993	7.51	1.84	0.29	85	25-500	square	1/X	0.9983	1/X	10	137	CE-UV [29]
<b>Dicarboxylic acids</b>													
Dimethylmalonate	131.035	17.78	0.86	1.14	105	1-250	square	1/X	0.9992	1/X	0.1	13	CE-MS [27]
Methylmalonate	117.019	18.25	1.25	0.37	97	5.0-500	square	1/X	0.9979	1/X	1	2	LC-MS [62]
Citraconate	129.019	18.30	2.08	1.31	98	2.5-500	linear	1/X	0.9988	1/X	0.25	0.4	IEC-MS [63]
Malonate	103.004	18.68	2.12	2.10	96	5-500	square	1/X	0.9982	1/X	0.5	1	IEC-MS [63]
Maleate	115.004	18.85	1.16	0.63	95	0.5-500	square	1/X	0.9989	1/X	0.25	0.1	HILIC-MS [64]
Glutarate	131.035	18.85	0.85	0.25	98	2.5-500	square	1/X	0.9983	1/X	0.25	1.7	HILIC-MS [64]
Malate	133.014	18.85	2.58	1.07	95	1-500	linear	1/X	0.9911	1/X	0.25	0.1	IEC-MS [63]
L-Tartrate	149.009	19.04	1.63	1.21	88	1-500	square	1/X	0.9991	1/X	0.5	20	LC-MS [65]
Tartronate	118.999	19.09	1.91	0.99	94	2.5-500	square	1/x	0.9996	1/x	0.5	-	-
Methylsuccinate	131.035	19.27	0.78	1.30	106	2.5-500	square	1/X	0.9965	1/X	0.5	40	CE-MS [27]
Succinate	117.019	19.36	2.15	0.09	105	10-500	square	1/X	0.9977	1/X	2.5	0.1	HILIC-MS [64]
Adipate	145.051	19.38	1.23	0.83	104	5-250	linear	1/X	0.9913	1/X	1	0.4	LC-MS [66]
Oxalate	88.988	19.40	0.81	0.74	116	5-250	linear	Equal	0.9904	Equal	1	18	IEC-MS [63]
Pimelate	159.066	19.77	1.42	1.37	100	5-500	linear	1/X	0.9991	1/X	1	0.09	HILIC-MS [64]
Suberate	173.082	20.54	1.94	1.07	103	10-500	linear	1/X	0.9988	1/X	2.5	0.03	HILIC-MS [64]
Mesaconate	129.019	21.53	1.53	2.03	97	5-500	square	1/X	0.9975	1/X	1	-	-
Azelate	187.098	21.58	1.52	0.17	110	5-500	linear	1/X	0.9968	1/X	1	0.03	HILIC-MS [64]
Fumarate	115.004	23.90	5.88	1.69	101	10-500	square	1/X <sup>2</sup>	0.9659	1/X <sup>2</sup>	2.5	0.9	LC-MS [62]

(Continues)

TABLE 1 (Continued)

Compound	Signal [M-H] <sup>-</sup> m/z	Repeatability		Recovery Polycarbonate filter 0.25 mL extraction %	Calibration		R <sup>2</sup>	Weighting function	Limit of detection		Method and reference for LOD comparison	
		RT (RSD) min %	Intraday (RSD) %		Interday (RSD) %	Calibration range µg L <sup>-1</sup>			Calibration function	LOD IC-MS µg L <sup>-1</sup>		LOD ref. ences µg L <sup>-1</sup>
<i>Tricarboxylic acids</i>												
Citrate	191.020	26.60	3.15	6.30	91	1-500	square	0.9948	1/X	0.5	0.4	IEC-MS [63]
<i>Terpene derived acids</i>												
Norpinonate	169.087	5.82	0.80	0.52	105	1-500	linear	0.9944	1/X	0.25	0.5	LC-MS [67]
Terebate	157.051	6.14	2.33	2.38	104	25-500	linear	0.9979	Equal	2.5	-	-
cis-Pinonate	183.103	6.23	0.99	0.50	98	1-500	linear	0.9959	1/X	0.1	1	LC-MS [67]
DTAA	231.087	18.73	1.12	0.62	98	1-250	square	0.9931	1/X	0.5	-	-
trans-Norpinate	171.066	18.92	1.13	0.44	93	10-250	square	0.9893	1/X	2.5	-	-
Pinate	185.082	19.27	1.59	0.43	95	5-250	linear	0.9954	1/X	1	0.1	HILIC-MS [64]
CA	199.098	19.30	1.13	1.16	93	1-250	linear	0.9989	1/X	0.25	-	-
MBTCA	203.056	26.66	1.18	1.47	90	2.5-500	linear	0.9994	Equal	0.25	0.1	LC-MS [66]
<i>Organosulfonates and -sulfates</i>												
MSA	94.981	6.57	0.67	0.24	104	5-500	linear	0.9953	Equal	1	40	CE-UV [61]
CSA	231.070	8.39	0.74	0.12	96	1-500	linear	0.9976	Equal	0.5	4.2	LC-MS [68]
LimonaketoneOS	251.059	8.68	1.11	1.04	99	1-500	square	0.9964	1/X	0.5	0.4	LC-MS [69]
Methylsulfate	110.976	10.01	0.85	0.31	100	0.5-500	square	0.9985	1/X	0.075	2.6	HILIC-MS [33]
HAS	152.986	10.10	0.82	0.75	107	0.25-500	linear	0.9972	1/X	0.075	2.6	HILIC-MS [33]
α-PineneOS	249.080	12.88	1.64	0.27	94	1-500	linear	0.9976	1/x	0.5	0.6	LC-MS [69]
CareneOS	249.080	14.52	1.31	2.35	97	0.5-500	linear	0.9978	1/X	0.25	0.5	LC-MS [69]
Mannose-6-sulfate	259.013	17.89	2.41	2.55	97	5-500	square	0.9972	1/X	2.5	-	-
Octylsulfate	209.085	32.54	1.25	0.80	92	2.5-500	linear	0.9992	Equal	1	2.4	LC-MS [68]

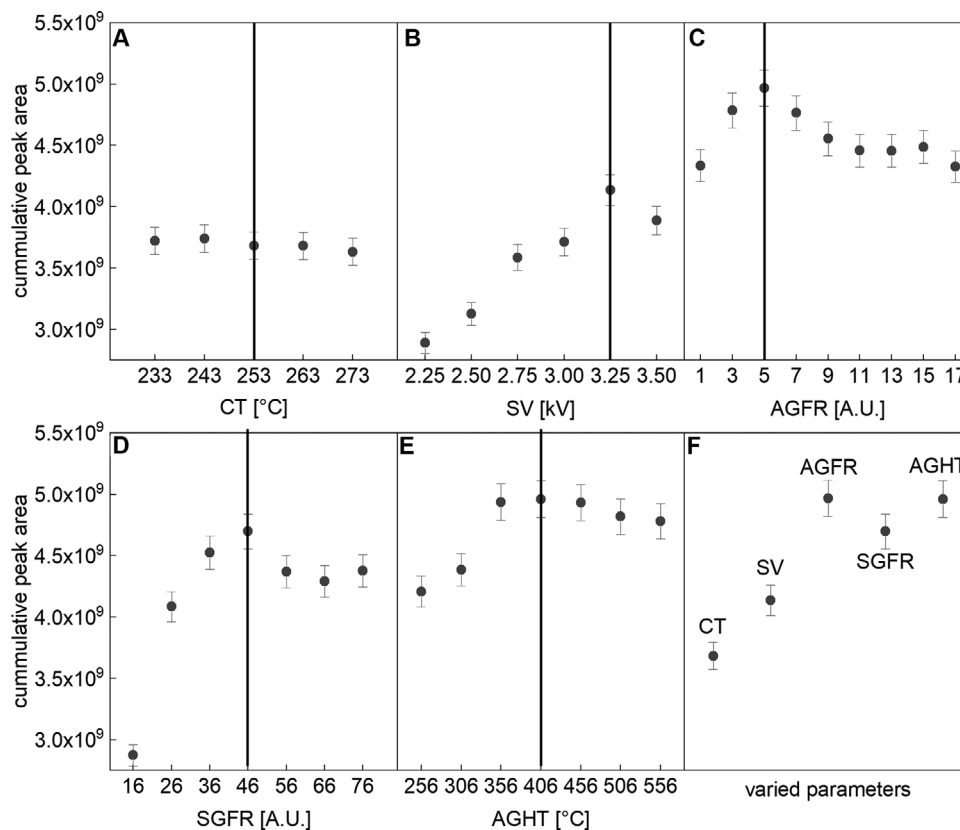


**FIGURE 4** Influence of the ESI source parameters (A) capillary temperature (CT), (B) spray voltage (SV), (C) aux gas flow rate (AGFR), (D) sheath gas flow rate (SGFR), (E) aux gas heater temperature (AGHT) on the cumulative peak area of all analytes. (F) All final parameters in the order of their optimization

the remaining compounds, LODs are nearly equal to the literature references. Even with low injection volumes of 5  $\mu\text{L}$ , compared to previously published methods the IC-MS could improve the detection for 22 compounds. Due to the low LODs, the filtered aqueous sample extraction can directly be injected. An error-prone and time-consuming further enrichment of the samples, e.g., with solid-phase extraction or the evaporation of excess solvent, is avoided. Accordingly, the method benefits from a minimal sample preparation before the measurement. Furthermore, the methods listed in Table 1 focus only on a few numbers of compounds and have difficulties especially with the analysis of organosulfates. Since LC-MS is used for the separation of larger organosulfates like limonaketoneOS,  $\alpha$ -pineneOS, and careneOS as well as the surrogates octylsulfate and CSA [68, 69], LC cannot properly separate small polar compounds. In contrast, organosulfates contained in samples with  $m/z > 200$  have difficulties to be baseline-resolved with HILIC-MS [33] and suffer under poor peak shape. Smaller compounds elute within the first minute near the dead volume and therefore can be suppressed by coeluting of a large number of other compounds. The method presented in this study is able to

baseline separate and detect all organosulfates and avoids suppression effects by early elution.

### 3.3 | Method application

With the developed IC-MS method three ambient particle samples from Melpitz and the arctic flight campaigns ACLOUD and PAMARCMiP 2018 were investigated. The corresponding chromatograms are shown in Supporting Information Figures S1–S3. The atmospheric concentrations of the observed analytes are listed in Table 2 and were calculated including a correction for field blank values. Typically, nitrate and sulfate are the main components of particle mass and showed the highest concentration in all samples. In addition, the samples from the rural background station in Melpitz show 2.7  $\text{ng m}^{-3}$  and the ACLOUD sample 0.2  $\text{ng m}^{-3}$  sulfite. Bromide was determined in all three samples with an average concentration of 0.9  $\text{ng m}^{-3}$ . In previous studies, bromide has been identified as an important component of sea salt aerosol [70, 71], arctic snow [72, 73], and cloud and fog samples of polluted air [74]. Besides the inorganic anions,

**TABLE 2** Results of ambient particle samples from three different sites. All concentrations are given in  $\text{ng m}^{-3}$ 

Compound	ACLOUD	Melpitz	PAMARCMiP
<b>Inorganic anions</b>			
Bromide	0.8	0.8	1.1
Nitrate	15	368	85
Sulfate	318	389	247
Sulfite	0.2	2.7	<blank
<b>Monocarboxylic acids</b>			
Glycolate	0.8	23.1	<blank
Pyruvate	4.5	12.0	<blank
Glyoxylate	n.d.	10.5	n.d.
<b>Dicarboxylic acids</b>			
Dimethylmalonate	n.d.	0.4	n.d.
Methylmalonate	n.d.	0.7	n.d.
Citraconate	n.d.	1.1	n.d.
Malonate	<blank	4.1	n.d.
Maleate	n.d.	3.8	n.d.
Glutarate	0.2	2.3	n.d.
Malate	0.6	<blank	n.d.
L-Tartrate	0.1	1.6	n.d.
Tartronate	0.7	5.0	n.d.
Methylsuccinate	n.d.	0.4	n.d.
Succinate	2.6	1.6	n.d.
Adipate	n.d.	0.3	5.3
Oxalate	1.5	98.2	<blank
Pimelate	<blank	<blank	6.9
Suberate	2.7	0.1	n.d.
Mesaconate	n.d.	n.d.	n.d.
Azelate	2.7	1.7	3.00
Fumarate	n.d.	0.8	n.d.
<b>Tricarboxylic acids</b>			
Citrate	n.d.	1.8	n.d.
<b>Terpene-derived acids</b>			
Norpinonate	n.d.	n.d.	n.d.
Terebate	1.6	3.0	n.d.
cis-Pinonate	1.0	n.d.	n.d.
DTAA	n.d.	0.2	n.d.
trans-Norpinate	n.d.	n.d.	n.d.
Pinate	n.d.	0.3	n.d.
CA	n.d.	n.d.	n.d.
MBTCA	1.5	1.1	n.d.
<b>Organosulfonates and -sulfates</b>			
MSA	17.8	4.5	<blank
CSA	n.d.	n.d.	n.d.
LimonaketoneOS	n.d.	n.d.	n.d.
Methylsulfate	<blank	0.3	n.d.

(Continues)

**TABLE 2** (Continued)

Compound	ACLOUD	Melpitz	PAMARCMiP
HAS	n.d.	0.6	n.d.
$\alpha$ -PineneOS	n.d.	n.d.	n.d.
CareneOS	n.d.	n.d.	n.d.
Mannose-6-sulfate	n.d.	n.d.	n.d.
Octylsulfate	n.d.	n.d.	n.d.

n.d.: not detected, &lt;blank: concentrations below the field blank values.

several organic tracers were identified and quantified. For the MCAs glycolate, pyruvate and glyoxylate, the concentrations of the Melpitz sample ranged from 10.5 to 23.1  $\text{ng m}^{-3}$ . Anthropogenic sources like the combustion of fossil fuels and the burning of biomass could be relevant sources for these compounds [3]. According to the authors' knowledge, MCAs, DCAs, MSA, and terpene-derived compounds could be determined for the first time from filter-based flight measurements in the arctic atmosphere. Pyruvic acid and glycolic acid were also determined in the sample from the ACLOUD campaign. Due to the flight path above Svalbard and the arctic ocean both compounds, as well as the detected DCAs oxalic, succinic, glutaric, suberic, and azelaic acid could be of rural and marine origin. Also hydroxylated diacids tartronic and tartaric acid were found in marine samples before [75] and might therefore be attributed to oceanic sources. Longer chain DCAs ( $C_5$ - $C_{12}$ ) are known to result from the photochemical oxidation of fatty acids found in the sea surface and can be oxidized to short chain DCAs ( $C_2$ - $C_4$ ) [76, 77]. Marine emission would also explain the determination of adipic acid, pimelic acid, and azelaic acid in the sample from the PAMARCMiP 2018 campaign. Besides, for the research station in Melpitz anthropogenic emissions and subsequent photochemical oxidations seem to be a possible explanation for the high variety of detected diacids [1], including low molecular weight DCAs ( $C_2$ - $C_4$ ), hydroxylated DCAs such as tartronic, tartaric and malic acid, as well as the unsaturated DCAs maleic and fumaric acid and branched DCAs such as methylmalonic, dimethylmalonic, and methylsuccinic acid, which are known to be formed by the oxidation of aromatic hydrocarbons [6, 42, 76] and methylcycloalkenes [78]. Citraconic acid has, to the best of the author's knowledge not yet been detected in atmospheric particles. The detection of the terpene derived acids MBTCA, terebic acid, pinic acid, and DTAA indicates a certain vegetative activity [10] and the emission of terpenes also during wintertime. Terebic acid, MBTCA, and cis-pinonic acid were also determined from the filter of the ACLOUD campaign. According to the literature [79], terpenoid compounds can correlate moderately with other tracers of biological activity in the ocean like MSA, that could also be quantified with 17.8  $\text{ng m}^{-3}$ . In

lower concentrations of  $4.6 \text{ ng m}^{-3}$  MSA was also found in the Melpitz sample. Further organosulfates were detected in the form of  $0.6 \text{ ng m}^{-3}$  HAS and  $0.3 \text{ ng m}^{-3}$  methylsulfate, which were both reported in urban areas before [33, 80]. Further organosulfates could not be detected or were below the field blank values of the samples.

## 4 | CONCLUSIONS

An IC-MS method was developed to determine organic acids, organosulfates, and inorganic anions in aqueous extracts of aerosol particles with high sensitivity. All compounds were separated within 33 min using an AS19-4  $\mu\text{m}$  column with a multi-step KOH gradient. To optimize sensitivity, the influence of organic post-column solvents, acidic as well as basic additives, and the ESI source parameters were investigated. The resulting method is characterized by a good inter- and intraday reproducibility below 3 %, recoveries in the range of 85–117 %, minimal sample preparation and was successfully applied to real samples. Compared to other methods that focus on specific tracers, a broad range of 43 compounds can be determined in a single run. LODs were improved for 22 compounds. In all samples both inorganic anions and MCAs could be detected. The sample from the ground station in Melpitz showed signals for all compound classes. In addition, it was also possible to identify aliphatic long-chain DCAs in the pure arctic air of the PAMARCMiP flight sample. Also, short-chain aliphatic and hydroxylated DCAs as well as terpene-derived acids and MSA could be observed in the sample from the ALOUD campaign. Thus, for the first time, a variety of organic tracers could be determined on arctic flight filters. In future studies, the new method will be applied to a larger set of ambient field samples to quantify concentrations of the described organic tracers and possibly also identify new compounds based on the high-resolution orbitrap MS capabilities.


## ACKNOWLEDGMENTS

We gratefully acknowledge the funding of S. Mertes by the Deutsche Forschungsgemeinschaft (DFG, German Research Foundation) – Project Number 268020496 – TRR 172, within the Transregional Collaborative Research Center “Arctic Amplification: Climate Relevant Atmospheric and Surface Processes, and Feedback Mechanisms (AC)<sup>3</sup>. Furthermore, we thank the DFG for funding the joint development of the HERA sampler under project Hera4HALO (FK HE 3086/31-1 and STR 453/10-1) supporting C. Kwiezinski and C. Jentsch and the subsequent funding of the projects HE 3086/44-1 and STR 453/13-1, which are both part of the DFG priority program HALO SPP 1294.

## CONFLICT OF INTEREST

The authors have declared no conflict of interest.

## ORCID

Martin Brüggemann  <https://orcid.org/0000-0003-2106-9691>

Hartmut Herrmann  <https://orcid.org/0000-0001-7044-2101>

## REFERENCES

- van Pinxteren D, Neusüß C, Herrmann H. On the abundance and source contributions of dicarboxylic acids in size-resolved aerosol particles at continental sites in central Europe. *Atmos. Chem. Phys.* 2014;14:3913–28.
- Brüggemann M, Xu R, Tilgner A, Kwong KC, Mutzel A, Poon HY, Otto T, Schaefer T, Poulain L, Chan MN, Herrmann H. Organosulfates in ambient aerosol: state of knowledge and future research directions on formation, abundance, fate, and importance. *Environ. Sci. Technol.* 2020;54:3767–82.
- Kawamura K, Tachibana E, Okuzawa K, Aggarwal SG, Kanaya Y, Wang ZF. High abundances of water-soluble dicarboxylic acids, ketocarboxylic acids and  $\alpha$ -dicarbonyls in the mountain-top aerosols over the North China Plain during wheat burning season. *Atmos. Chem. Phys.* 2013;13:8285–302.
- Limbeck A, Puxbaum H. Organic acids in continental background aerosols. *Atmos. Environ.* 1999;33:1847–52.
- Kawamura K, Bikkina S. A review of dicarboxylic acids and related compounds in atmospheric aerosols: Molecular distributions, sources and transformation. *Atmos. Res.* 2016;170:140–60.
- Röhl A, Lammel G. Determination of malic acid and other C4 dicarboxylic acids in atmospheric aerosol samples. *Chemosphere.* 2002;46:1195–9.
- Liu Y, Monod A, Tritscher T, Praplan AP, DeCarlo PF, Temime-Roussel B, Quivet E, Marchand N, Dommen J, Baltensperger U. Aqueous phase processing of secondary organic aerosol from isoprene photooxidation. *Atmos. Chem. Phys.* 2012;12:5879–95.
- Warneck P. In-cloud chemistry opens pathway to the formation of oxalic acid in the marine atmosphere. *Atmos. Environ.* 2003;37:2423–7.
- Carlton AG, Wiedinmyer C, Kroll JH. A review of secondary organic aerosol (SOA) formation from isoprene. *Atmos. Chem. Phys.* 2009;9:8261–305.
- Larsen BR, Lahaniati M, Calogirou A, Kotzias D. Atmospheric oxidation products of terpenes: A new nomenclature. *Chemosphere.* 1998;37:1207–20.
- Passananti M, Kong L, Shang J, Dupart Y, Perrier S, Chen J, Donaldson DJ, George C. Organosulfate formation through the heterogeneous reaction of sulfur dioxide with unsaturated fatty acids and long-chain alkenes. *Angew. Chem. Int. Ed.* 2016;55:10336–9.
- Iinuma Y, Müller C, Berndt T, Bøge O, Claeys M, Herrmann H. Evidence for the existence of organosulfates from  $\beta$ -pinene ozonolysis in ambient secondary organic aerosol. *Environ. Sci. Technol.* 2007;41:6678–83.
- Iinuma Y, Müller C, Bøge O, Gnauk T, Herrmann H. The formation of organic sulfate esters in the limonene ozonolysis secondary organic aerosol (SOA) under acidic conditions. *Atmos. Environ.* 2007;41:5571–83.

14. Surratt JD, Gomez-Gonzalez Y, Chan AW, Vermeylen R, Shahgholi M, Kleindienst TE, Edney EO, Offenberg JH, Lewandowski M, Jaoui M, Maenhaut W, Claeys M, Flagan RC, Seinfeld JH. Organosulfate formation in biogenic secondary organic aerosol. *J. Phys. Chem. A*. 2008;112:8345–78.
15. Surratt JD, Chan AW, Eddingsaas NC, Chan M, Loza CL, Kwan AJ, Hersey SP, Flagan RC, Wennberg PO, Seinfeld JH. Reactive intermediates revealed in secondary organic aerosol formation from isoprene. *Proc. Natl. Acad. Sci. U. S. A.* 2010;107:6640–5.
16. Brock CA, Radke LF, Lyons JH, Hobbs PV. Arctic hazes in summer over Greenland and the North American Arctic. I: Incidence and origins. *J. Atmos. Chem.* 1989;9:129–48.
17. Li S-M, Winchester JW. Aerosol silicon and associated elements in the arctic high and mid-troposphere. *Atmos. Environ., Part A*. 1993;27:2907–12.
18. Sheridan PJ, Zoller WH. Elemental composition of particulate material sampled from the Arctic haze aerosol. *J. Atmos. Chem.* 1989;9:363–81.
19. Visentin M, Pietrogrande MC. Determination of polar organic compounds in atmospheric aerosols by gas chromatography with ion trap tandem mass spectrometry. *J. Sep. Sci.* 2014;37:1561–9.
20. Teich M, Schmidpott M, van Pinxteren D, Chen J, Herrmann H. Separation and quantification of imidazoles in atmospheric particles using LC-Orbitrap-MS. *J. Sep. Sci.* 2020;43:577–89.
21. Domingos JS, Regis AC, Santos JV, de Andrade JB, da Rocha GO. A comprehensive and suitable method for determining major ions from atmospheric particulate matter matrices. *J. Chromatogr. A*. 2012;1266:17–23.
22. Dabek-Zlotorzynska E, Aranda-Rodriguez R, Graham L. Capillary electrophoresis determinative and GC-MS confirmatory method for water-soluble organic acids in airborne particulate matter and vehicle emission. *J. Sep. Sci.* 2005;28:1520–8.
23. Kawamura K, Ikushima K. Seasonal changes in the distribution of dicarboxylic acids in the urban atmosphere. *Environ. Sci. Technol.* 1993;27:2227–35.
24. Limbeck A, Puxbaum H. A GC-MS method for the determination of polar organic compounds in atmospheric samples. *Int. J. Environ. Anal. Chem.* 1999;73:329–43.
25. van Pinxteren D, Teich M, Herrmann H. Hollow fibre liquid-phase microextraction of functionalised carboxylic acids from atmospheric particles combined with capillary electrophoresis/mass spectrometric analysis. *J. Chromatogr. A*. 2012;1267:178–88.
26. Brudin SS, Shellie RA, Haddad PR, Schoenmakers PJ. Comprehensive two-dimensional liquid chromatography: ion chromatography  $\times$  reversed-phase liquid chromatography for separation of low-molar-mass organic acids. *J. Chromatogr. A*. 2010;1217:6742–6.
27. van Pinxteren D, Herrmann H. Determination of functionalised carboxylic acids in atmospheric particles and cloud water using capillary electrophoresis/mass spectrometry. *J. Chromatogr. A*. 2007;1171:112–23.
28. Adler H, Siren H. Study on dicarboxylic acids in aerosol samples with capillary electrophoresis. *J. Anal. Methods Chem.* 2014;2014:498168.
29. Dabek-Zlotorzynska E, Piechowski M, McGrath M, Lai EPC. Determination of low-molecular-mass carboxylic acids in atmospheric aerosol and vehicle emission samples by capillary electrophoresis. *J. Chromatogr. A*. 2001;910:331–45.
30. Yassine MM, Dabek-Zlotorzynska E, Harir M, Schmitt-Kopplin P. Identification of weak and strong organic acids in atmospheric aerosols by capillary electrophoresis/mass spectrometry and ultra-high-resolution fourier transform ion cyclotron resonance mass spectrometry. *Anal. Chem.* 2012;84:6586–94.
31. Kristensen K, Glasius M. Organosulfates and oxidation products from biogenic hydrocarbons in fine aerosols from a forest in North West Europe during spring. *Atmos. Environ.* 2011;45:4546–56.
32. Cui T, Zeng Z, Dos Santos EO, Zhang Z, Chen Y, Zhang Y, Rose CA, Budisulistiorini SH, Collins LB, Bodnar WM, de Souza RAF, Martin ST, Machado CMD, Turpin BJ, Gold A, Ault AP, Surratt JD. Development of a hydrophilic interaction liquid chromatography (HILIC) method for the chemical characterization of water-soluble isoprene epoxydiol (IEPOX)-derived secondary organic aerosol. *Environ. Sci.: Processes Impacts*. 2018;20:1524–36.
33. Hettiyadura APS, Stone EA, Kundu S, Baker Z, Geddes E, Richards K, Humphry T. Determination of atmospheric organosulfates using HILIC chromatography with MS detection. *Atmos. Meas. Tech.* 2015;8:2347–58.
34. Nguyen HP, Schug KA. The advantages of ESI-MS detection in conjunction with HILIC mode separations: Fundamentals and applications. *J. Sep. Sci.* 2008;31:1465–80.
35. Guo Y, Gaiki S. Retention behavior of small polar compounds on polar stationary phases in hydrophilic interaction chromatography. *J. Chromatogr. A*. 2005;1074:71–80.
36. Alpert AJ. Effect of salts on retention in hydrophilic interaction chromatography. *J. Chromatogr. A*. 2018;1538:45–53.
37. Knepper TP, Werner A, Bogenschütz G. Determination of synthetic chelating agents in surface and waste water by ion chromatography-mass spectrometry. *J. Chromatogr. A*. 2005;1085:240–6.
38. Panseri S, Nobile M, Arioli F, Biolatti C, Pavlovic R, Chiesa LM. Occurrence of perchlorate, chlorate and polar herbicides in different baby food commodities. *Food Chem.* 2020;330:127205.
39. Barron L, Gilchrist E. Ion chromatography-mass spectrometry: A review of recent technologies and applications in forensic and environmental explosives analysis. *Anal. Chim. Acta*. 2014;806:27–54.
40. Baygildiev T, Vokuev M, Ogorodnikov R, Braun A, Rybalchenko I, Rodin I. Simultaneous determination of organophosphorus nerve agent markers in urine by IC-MS/MS using anion-exchange solid-phase extraction. *J. Chromatogr. B: Anal. Technol. Biomed. Life Sci.* 2019;1132:121815.
41. Jansons M, Pugajeva I, Bartkevics V. Evaluation of selected buffers for simultaneous determination of ionic and acidic pesticides including glyphosate using anion exchange chromatography with mass spectrometric detection. *J. Sep. Sci.* 2019;42:3077–85.
42. Fisseha R, Dommen J, Sax M, Paulsen D, Kalberer M, Maurer R, Hofler F, Weingartner E, Baltensperger U. Identification of organic acids in secondary organic aerosol and the corresponding gas phase from chamber experiments. *Anal. Chem.* 2004;76:6535–40.

43. Boring CB, Al-Horr R, Genfa Z, Dasgupta PK, Martin MW, Smith WF. Field measurement of acid gases and soluble anions in atmospheric particulate matter using a parallel plate wet denuder and an alternating filter-based automated analysis system. *Anal. Chem.* 2002;74:1256–68.
44. Wendisch M, Macke A, Ehrlich A, Lüpkes C, Mech M, Chechin D, Dethloff K, Velasco CB, Bozem H, Brückner M, Clemen H-C, Crewell S, Donth T, Dupuy R, Ebell K, Egerer U, Engelmann R, Engler C, Eppers O, Gehrman M, Gong X, Gottschalk M, Goubeyre C, Griesche H, Hartmann J, Hartmann M, Heinold B, Herber A, Herrmann H, Heygster G, Hoor P, Jafariserajehlou S, Jäkel E, Järvinen E, Jourdan O, Kästner U, Kecorius S, Knudsen EM, Köllner F, Kretschmar J, Lelli L, Leroy D, Maturilli M, Mei L, Mertes S, Mioche G, Neuber R, Nicolaus M, Nomokonova T, Notholt J, Palm M, van Pinxteren M, Quaas J, Richter P, Ruiz-Donoso E, Schäfer M, Schmieder K, Schnaiter M, Schneider J, Schwarzenböck A, Seifert P, Shupe MD, Siebert H, Spreen G, Stapf J, Stratmann F, Vogl T, Welti A, Wex H, Wiedensohler A, Zannata M, Zeppenfeld S. The Arctic cloud puzzle: using A-Cloud/PASCAL multiplatform observations to unravel the role of clouds and aerosol particles in Arctic amplification. *Bull. Am. Meteorol. Soc.* 2019;100:841–71.
45. Ehrlich A, Wendisch M, Lüpkes C, Buschmann M, Bozem H, Chechin D, Clemen H-C, Dupuy R, Eppers O, Hartmann J, Herber A, Jäkel E, Järvinen E, Jourdan O, Kästner U, Kliesch L-L, Köllner F, Mech M, Mertes S, Neuber R, Ruiz-Donoso E, Schnaiter M, Schneider J, Stapf J, Zannata M. A comprehensive in situ and remote sensing data set from the Arctic CLOUD Observations Using airborne measurements during polar Day (A-Cloud) campaign. *Earth Syst. Sci. Data.* 2019;11:1853–81.
46. Hartmann M, Adachi K, Eppers O, Haas C, Herber A, Holzinger R, Hünerbein A, Jäkel E, Jentsch C, Pinxteren M, Wex H, Willmes S, Stratmann F. Wintertime airborne measurements of ice nucleating particles in the high Arctic: a hint to a marine, biogenic source for ice nucleating particles. *Geophys. Res. Lett.* 2020;47.
47. Smith JN, Flagan RC, Beauchamp JL. Droplet evaporation and discharge dynamics in electrospray ionization. *J. Phys. Chem. A.* 2002;106:9957–67.
48. Mawhinney DB, Stanelle RD, Hamelin EI, Kobelski RJ. Enhancing the response of alkyl methylphosphonic acids in negative electrospray ionization liquid chromatography tandem mass spectrometry by post-column addition of organic solvents. *J. Am. Soc. Mass. Spectrom.* 2007;18:1821–6.
49. Amad MH, Cech NB, Jackson GS, Enke CG. Importance of gas-phase proton affinities in determining the electrospray ionization response for analytes and solvents. *J. Mass Spectrom.* 2000;35:784–9.
50. Hopfgartner G, Bean K, Henion J, Henry R. Ion spray mass spectrometric detection for liquid chromatography: a concentration- or a mass-flow-sensitive device?. *J. Chromatogr.* 1993;647:51–61.
51. Vestal ML, in: Standing, K. G., Ens, W. (Eds.), *Methods and Mechanisms for Producing Ions from Large Molecules*. Springer US, Boston, MA 1991, pp. 157–70.
52. Fernandez de la Mora J, R.-L J, *ASMS Conference on Mass Spectrometry and Allied Topics* Nashville 1991, pp. 441–2.
53. Straub RF, Voyksner RD. Negative ion formation in electrospray mass spectrometry. *J. Am. Soc. Mass. Spectrom.* 1993;4:578–87.
54. Beaudry F, Vachon P. Electrospray ionization suppression, a physical or a chemical phenomenon?. *Biomed. Chromatogr.* 2006;20:200–5.
55. Kebarle P, Verkerk UH. Electrospray: From ions in solution to ions in the gas phase, what we know now. *Mass Spectrom. Rev.* 2009;28:898–917.
56. Bruins AP, Covey TR, Henion JD. Ion spray interface for combined liquid chromatography/atmospheric pressure ionization mass spectrometry. *Anal. Chem.* 1987;59:2642–6.
57. Fenn JB. Ion formation from charged droplets: roles of geometry, energy, and time. *J. Am. Soc. Mass. Spectrom.* 1993;4:524–35.
58. Fosco T, Schmeling M. Determination of water-soluble atmospheric aerosols using ion chromatography. *Environ. Monit. Assess.* 2007;130:187–99.
59. Zuo Y, Wang C, Van T. Simultaneous determination of nitrite and nitrate in dew, rain, snow and lake water samples by ion-pair high-performance liquid chromatography. *Talanta.* 2006;70:281–5.
60. Zuo Y, Chen H. Simultaneous determination of sulfite, sulfate, and hydroxymethanesulfonate in atmospheric waters by ion-pair HPLC technique. *Talanta.* 2003;59:875–81.
61. Gao S, Rudolph J. Measurements of low-molecular-mass carboxylic acids in atmospheric aerosols by capillary electrophoresis. *J. Chromatogr. Sci.* 2004;42:323–8.
62. Marquis BJ, Louks HP, Bose C, Wolfe RR, Singh SP. A new derivatization reagent for HPLC-MS analysis of biological organic acids. *Chromatographia.* 2017;80:1723–32.
63. Bylund D, Norstrom SH, Essen SA, Lundstrom US. Analysis of low molecular mass organic acids in natural waters by ion exclusion chromatography tandem mass spectrometry. *J. Chromatogr. A.* 2007;1176:89–93.
64. Kitanovski Z, Grgic I, Veber M. Characterization of carboxylic acids in atmospheric aerosols using hydrophilic interaction liquid chromatography tandem mass spectrometry. *J. Chromatogr. A.* 2011;1218:4417–25.
65. Chen Z, Jin X, Wang Q, Lin Y, Gan L, Tang C. Confirmation and determination of carboxylic acids in root exudates using LC-ESI-MS. *J. Sep. Sci.* 2007;30:2440–6.
66. Zhang YY, Müller L, Winterhalter R, Moortgat GK, Hoffmann T, Pöschl U. Seasonal cycle and temperature dependence of pinene oxidation products, dicarboxylic acids and nitrophenols in fine and coarse air particulate matter. *Atmos. Chem. Phys.* 2010;10:7859–73.
67. Warnke J, Bandur R, Hoffmann T. Capillary-HPLC-ESI-MS/MS method for the determination of acidic products from the oxidation of monoterpenes in atmospheric aerosol samples. *Anal. Bioanal. Chem.* 2006;385:34–45.
68. Wang Y, Ren J, Huang XHH, Tong R, Yu JZ. Synthesis of four monoterpene-derived organosulfates and their quantification in atmospheric aerosol samples. *Environ. Sci. Technol.* 2017;51:6791–801.
69. Wang Y, Ma Y, Li X, Kuang BY, Huang C, Tong R, Yu JZ. Monoterpene and sesquiterpene  $\alpha$ -hydroxy organosulfates: synthesis, MS/MS characteristics, and ambient presence. *Environ. Sci. Technol.* 2019;53:12278–90.
70. Ayers GP, Gillett RW, Caine JM, Dick AL. Chloride and bromide depletions in sea-salt particles over the northeastern Pacific Ocean. *J. Atmos. Chem.* 1999;33:299–319.

71. Gabriel R. Bromide content of sea-salt aerosol particles collected over the Indian Ocean during INDOEX 1999. *J. Geophys. Res.* 2002;107.
72. Krnavek L, Simpson WR, Carlson D, Domine F, Douglas TA, Sturm M. The chemical composition of surface snow in the Arctic: Examining marine, terrestrial, and atmospheric influences. *Atmos. Environ.* 2012;50:349–59.
73. Simpson WR, Alvarez-Aviles L, Douglas TA, Sturm M, Domine F. Halogens in the coastal snow pack near Barrow, Alaska: Evidence for active bromine air-snow chemistry during springtime. *Geophys. Res. Lett.* 2005;32:1–4.
74. Lammel G. Particulate and fog- and cloud-water bromide in polluted air. *Atmos. Environ.* 1995;29:3257–62.
75. Gowda D, Kawamura K, Tachibana E. Identification of hydroxy- and keto-dicarboxylic acids in remote marine aerosols using gas chromatography/quadrupole and time-of-flight mass spectrometry. *Rapid Commun. Mass Spectrom.* 2016;30:992–1000.
76. Kawamura K, Kasukabe H, Barrie LA. Source and reaction pathways of dicarboxylic acids, ketoacids and dicarbonyls in arctic aerosols: One year of observations. *Atmos. Environ.* 1996;30:1709–22.
77. Tedetti M, Kawamura K, Narukawa M, Joux F, Charrière B, Sempéré R. Hydroxyl radical-induced photochemical formation of dicarboxylic acids from unsaturated fatty acid (oleic acid) in aqueous solution. *J. Photochem. Photobiol. A.* 2007;188:135–9.
78. Grosjean D, Fung K. Hydrocarbons and carbonyls in Los Angeles air. *J. Air Pollut. Control Assoc.* 1984;34:537–43.
79. Cui T, Green HS, Selleck PW, Zhang Z, O'Brien RE, Gold A, Keywood M, Kroll JH, Surratt JD. Chemical characterization of isoprene- and monoterpene-derived secondary organic aerosol tracers in remote marine aerosols over a quarter century. *ACS Earth Space Chem.* 2019;3:935–46.
80. Huang R-J, Cao J, Chen Y, Yang L, Shen J, You Q, Wang K, Lin C, Xu W, Gao B, Li Y, Chen Q, Hoffmann T, Bilde M, Glasius M, Dörmann M, Sjöström A, Wahner A, Williams PI, Wu Y, Xiao F, Zhang Y, Zhou W, Ziehm R, Shi X, Han Y, He H, Hu M, Iinuma Y, Kang S, Kim S, Kirchner J, Li J, Liu T, Liu X, Luo J, Ma B, Manolopoulos S, Meng G, Mo H, Müller T, Nenes A, Ni J, Nishino K, Nothmann M, O'Donoghue M, Park J, Park M, Park S, Park T, Park Y, Paoli J, Perron M, Pilorgio G, Rissanen M, Salcedo A, Schill W, Shi X, Song M, Sun J, Sun Y, Sun Z, Tang M, Tölgel M, Tuohimäki M, Ullrich M, Wang L, Wang X, Wang Y, Wang Z, Wehner M, Whittaker L, Wu J, Wu J, Wu K, Wu X, Wu Y, Wu Z, Xiao F, Xie P, Xu L, Xu S, Xu T, Yamamoto Y, Yang G, Yang H, Yang L, Yang M, Yang Q, Yang S, Yang X, Yang Y, Yang Z, Yin H, Yin L, Yin X, Yin Y, Yin Z, Yu J, Yu K, Yu L, Yu S, Yu T, Yu W, Yu X, Yu Y, Yu Z, Zhang H, Zhang J, Zhang L, Zhang M, Zhang Q, Zhang R, Zhang S, Zhang T, Zhang W, Zhang X, Zhang Y, Zhang Z, Zhao J, Zhao M, Zhao Q, Zhao R, Zhao S, Zhao T, Zhao W, Zhao X, Zhao Y, Zhao Z, Zheng H, Zheng J, Zheng L, Zheng M, Zheng Q, Zheng R, Zheng S, Zheng T, Zheng W, Zheng X, Zheng Y, Zheng Z, Zhou H, Zhou J, Zhou L, Zhou M, Zhou Q, Zhou R, Zhou S, Zhou T, Zhou W, Zhou X, Zhou Y, Zhou Z, Zhu H, Zhu J, Zhu L, Zhu M, Zhu Q, Zhu R, Zhu S, Zhu T, Zhu W, Zhu X, Zhu Y, Zhu Z, Zieger W, Ziehm R, Ziehm S, Ziehm T, Ziehm W, Ziehm X, Ziehm Y, Ziehm Z, Ziehm A, Ziehm B, Ziehm C, Ziehm D, Ziehm E, Ziehm F, Ziehm G, Ziehm H, Ziehm I, Ziehm J, Ziehm K, Ziehm L, Ziehm M, Ziehm N, Ziehm O, Ziehm P, Ziehm Q, Ziehm R, Ziehm S, Ziehm T, Ziehm U, Ziehm V, Ziehm W, Ziehm X, Ziehm Y, Ziehm Z, Ziehm AA, Ziehm AB, Ziehm AC, Ziehm AD, Ziehm AE, Ziehm AF, Ziehm AG, Ziehm AH, Ziehm AI, Ziehm AJ, Ziehm AK, Ziehm AL, Ziehm AM, Ziehm AN, Ziehm AO, Ziehm AP, Ziehm AQ, Ziehm AR, Ziehm AS, Ziehm AT, Ziehm AU, Ziehm AV, Ziehm AW, Ziehm AX, Ziehm AY, Ziehm AZ, Ziehm BA, Ziehm BB, Ziehm BC, Ziehm BD, Ziehm BE, Ziehm BF, Ziehm BG, Ziehm BH, Ziehm BI, Ziehm BJ, Ziehm BK, Ziehm BL, Ziehm BM, Ziehm BN, Ziehm BO, Ziehm BP, Ziehm BQ, Ziehm BR, Ziehm BS, Ziehm BT, Ziehm BU, Ziehm BV, Ziehm BW, Ziehm BX, Ziehm BY, Ziehm BZ, Ziehm CA, Ziehm CB, Ziehm CC, Ziehm CD, Ziehm CE, Ziehm CF, Ziehm CG, Ziehm CH, Ziehm CI, Ziehm CJ, Ziehm CK, Ziehm CL, Ziehm CM, Ziehm CN, Ziehm CO, Ziehm CP, Ziehm CQ, Ziehm CR, Ziehm CS, Ziehm CT, Ziehm CU, Ziehm CV, Ziehm CW, Ziehm CX, Ziehm CY, Ziehm CZ, Ziehm DA, Ziehm DB, Ziehm DC, Ziehm DD, Ziehm DE, Ziehm DF, Ziehm DG, Ziehm DH, Ziehm DI, Ziehm DJ, Ziehm DK, Ziehm DL, Ziehm DM, Ziehm DN, Ziehm DO, Ziehm DP, Ziehm DQ, Ziehm DR, Ziehm DS, Ziehm DT, Ziehm DU, Ziehm DV, Ziehm DW, Ziehm DX, Ziehm DY, Ziehm DZ, Ziehm EA, Ziehm EB, Ziehm EC, Ziehm ED, Ziehm EE, Ziehm EF, Ziehm EG, Ziehm EH, Ziehm EI, Ziehm EJ, Ziehm EK, Ziehm EL, Ziehm EM, Ziehm EN, Ziehm EO, Ziehm EP, Ziehm EQ, Ziehm ER, Ziehm ES, Ziehm ET, Ziehm EU, Ziehm EV, Ziehm EW, Ziehm EX, Ziehm EY, Ziehm EZ, Ziehm FA, Ziehm FB, Ziehm FC, Ziehm FD, Ziehm FE, Ziehm FF, Ziehm FG, Ziehm FH, Ziehm FI, Ziehm FJ, Ziehm FK, Ziehm FL, Ziehm FM, Ziehm FN, Ziehm FO, Ziehm FP, Ziehm FQ, Ziehm FR, Ziehm FS, Ziehm FT, Ziehm FU, Ziehm FV, Ziehm FW, Ziehm FX, Ziehm FY, Ziehm FZ, Ziehm GA, Ziehm GB, Ziehm GC, Ziehm GD, Ziehm GE, Ziehm GF, Ziehm GG, Ziehm GH, Ziehm GI, Ziehm GJ, Ziehm GK, Ziehm GL, Ziehm GM, Ziehm GN, Ziehm GO, Ziehm GP, Ziehm GQ, Ziehm GR, Ziehm GS, Ziehm GT, Ziehm GU, Ziehm GV, Ziehm GW, Ziehm GX, Ziehm GY, Ziehm GZ, Ziehm HA, Ziehm HB, Ziehm HC, Ziehm HD, Ziehm HE, Ziehm HF, Ziehm HG, Ziehm HH, Ziehm HI, Ziehm HJ, Ziehm HK, Ziehm HL, Ziehm HM, Ziehm HN, Ziehm HO, Ziehm HP, Ziehm HQ, Ziehm HR, Ziehm HS, Ziehm HT, Ziehm HU, Ziehm HV, Ziehm HW, Ziehm HX, Ziehm HY, Ziehm HZ, Ziehm IA, Ziehm IB, Ziehm IC, Ziehm ID, Ziehm IE, Ziehm IF, Ziehm IG, Ziehm IH, Ziehm II, Ziehm IJ, Ziehm IK, Ziehm IL, Ziehm IM, Ziehm IN, Ziehm IO, Ziehm IP, Ziehm IQ, Ziehm IR, Ziehm IS, Ziehm IT, Ziehm IU, Ziehm IV, Ziehm IW, Ziehm IX, Ziehm IY, Ziehm IZ, Ziehm JA, Ziehm JB, Ziehm JC, Ziehm JD, Ziehm JE, Ziehm JF, Ziehm JG, Ziehm JH, Ziehm JI, Ziehm JJ, Ziehm JK, Ziehm JL, Ziehm JM, Ziehm JN, Ziehm JO, Ziehm JP, Ziehm JQ, Ziehm JR, Ziehm JS, Ziehm JT, Ziehm JU, Ziehm JV, Ziehm JW, Ziehm JX, Ziehm JY, Ziehm JZ, Ziehm KA, Ziehm KB, Ziehm KC, Ziehm KD, Ziehm KE, Ziehm KF, Ziehm KG, Ziehm KH, Ziehm KI, Ziehm KJ, Ziehm KK, Ziehm KL, Ziehm KM, Ziehm KN, Ziehm KO, Ziehm KP, Ziehm KQ, Ziehm KR, Ziehm KS, Ziehm KT, Ziehm KU, Ziehm KV, Ziehm KW, Ziehm KX, Ziehm KY, Ziehm KZ, Ziehm LA, Ziehm LB, Ziehm LC, Ziehm LD, Ziehm LE, Ziehm LF, Ziehm LG, Ziehm LH, Ziehm LI, Ziehm LJ, Ziehm LK, Ziehm LL, Ziehm LM, Ziehm LN, Ziehm LO, Ziehm LP, Ziehm LQ, Ziehm LR, Ziehm LS, Ziehm LT, Ziehm LU, Ziehm LV, Ziehm LW, Ziehm LX, Ziehm LY, Ziehm LZ, Ziehm MA, Ziehm MB, Ziehm MC, Ziehm MD, Ziehm ME, Ziehm MF, Ziehm MG, Ziehm MH, Ziehm MI, Ziehm MJ, Ziehm MK, Ziehm ML, Ziehm MM, Ziehm MN, Ziehm MO, Ziehm MP, Ziehm MQ, Ziehm MR, Ziehm MS, Ziehm MT, Ziehm MU, Ziehm MV, Ziehm MW, Ziehm MX, Ziehm MY, Ziehm MZ, Ziehm NA, Ziehm NB, Ziehm NC, Ziehm ND, Ziehm NE, Ziehm NF, Ziehm NG, Ziehm NH, Ziehm NI, Ziehm NJ, Ziehm NK, Ziehm NL, Ziehm NM, Ziehm NN, Ziehm NO, Ziehm NP, Ziehm NQ, Ziehm NR, Ziehm NS, Ziehm NT, Ziehm NU, Ziehm NV, Ziehm NW, Ziehm NX, Ziehm NY, Ziehm NZ, Ziehm OA, Ziehm OB, Ziehm OC, Ziehm OD, Ziehm OE, Ziehm OF, Ziehm OG, Ziehm OH, Ziehm OI, Ziehm OJ, Ziehm OK, Ziehm OL, Ziehm OM, Ziehm ON, Ziehm OO, Ziehm OP, Ziehm OQ, Ziehm OR, Ziehm OS, Ziehm OT, Ziehm OU, Ziehm OV, Ziehm OW, Ziehm OX, Ziehm OY, Ziehm OZ, Ziehm PA, Ziehm PB, Ziehm PC, Ziehm PD, Ziehm PE, Ziehm PF, Ziehm PG, Ziehm PH, Ziehm PI, Ziehm PJ, Ziehm PK, Ziehm PL, Ziehm PM, Ziehm PN, Ziehm PO, Ziehm PP, Ziehm PQ, Ziehm PR, Ziehm PS, Ziehm PT, Ziehm PU, Ziehm PV, Ziehm PW, Ziehm PX, Ziehm PY, Ziehm PZ, Ziehm QA, Ziehm QB, Ziehm QC, Ziehm QD, Ziehm QE, Ziehm QF, Ziehm QG, Ziehm QH, Ziehm QI, Ziehm QJ, Ziehm QK, Ziehm QL, Ziehm QM, Ziehm QN, Ziehm QO, Ziehm QP, Ziehm QQ, Ziehm QR, Ziehm QS, Ziehm QT, Ziehm QU, Ziehm QV, Ziehm QW, Ziehm QX, Ziehm QY, Ziehm QZ, Ziehm RA, Ziehm RB, Ziehm RC, Ziehm RD, Ziehm RE, Ziehm RF, Ziehm RG, Ziehm RH, Ziehm RI, Ziehm RJ, Ziehm RK, Ziehm RL, Ziehm RM, Ziehm RN, Ziehm RO, Ziehm RP, Ziehm RQ, Ziehm RR, Ziehm RS, Ziehm RT, Ziehm RU, Ziehm RV, Ziehm RW, Ziehm RX, Ziehm RY, Ziehm RZ, Ziehm SA, Ziehm SB, Ziehm SC, Ziehm SD, Ziehm SE, Ziehm SF, Ziehm SG, Ziehm SH, Ziehm SI, Ziehm SJ, Ziehm SK, Ziehm SL, Ziehm SM, Ziehm SN, Ziehm SO, Ziehm SP, Ziehm SQ, Ziehm SR, Ziehm SS, Ziehm ST, Ziehm SU, Ziehm SV, Ziehm SW, Ziehm SX, Ziehm SY, Ziehm SZ, Ziehm TA, Ziehm TB, Ziehm TC, Ziehm TD, Ziehm TE, Ziehm TF, Ziehm TG, Ziehm TH, Ziehm TI, Ziehm TJ, Ziehm TK, Ziehm TL, Ziehm TM, Ziehm TN, Ziehm TO, Ziehm TP, Ziehm TQ, Ziehm TR, Ziehm TS, Ziehm TT, Ziehm TU, Ziehm TV, Ziehm TW, Ziehm TX, Ziehm TY, Ziehm TZ, Ziehm UA, Ziehm UB, Ziehm UC, Ziehm UD, Ziehm UE, Ziehm UF, Ziehm UG, Ziehm UH, Ziehm UI, Ziehm UJ, Ziehm UK, Ziehm UL, Ziehm UM, Ziehm UN, Ziehm UO, Ziehm UP, Ziehm UQ, Ziehm UR, Ziehm US, Ziehm UT, Ziehm UU, Ziehm UV, Ziehm UW, Ziehm UX, Ziehm UY, Ziehm UZ, Ziehm VA, Ziehm VB, Ziehm VC, Ziehm VD, Ziehm VE, Ziehm VF, Ziehm VG, Ziehm VH, Ziehm VI, Ziehm VJ, Ziehm VK, Ziehm VL, Ziehm VM, Ziehm VN, Ziehm VO, Ziehm VP, Ziehm VQ, Ziehm VR, Ziehm VS, Ziehm VT, Ziehm VU, Ziehm VV, Ziehm VW, Ziehm VX, Ziehm VY, Ziehm VZ, Ziehm WA, Ziehm WB, Ziehm WC, Ziehm WD, Ziehm WE, Ziehm WF, Ziehm WG, Ziehm WH, Ziehm WI, Ziehm WJ, Ziehm WK, Ziehm WL, Ziehm WM, Ziehm WN, Ziehm WO, Ziehm WP, Ziehm WQ, Ziehm WR, Ziehm WS, Ziehm WT, Ziehm WU, Ziehm WV, Ziehm WW, Ziehm WX, Ziehm WY, Ziehm WZ, Ziehm XA, Ziehm XB, Ziehm XC, Ziehm XD, Ziehm XE, Ziehm XF, Ziehm XG, Ziehm XH, Ziehm XI, Ziehm XJ, Ziehm XK, Ziehm XL, Ziehm XM, Ziehm XN, Ziehm XO, Ziehm XP, Ziehm XQ, Ziehm XR, Ziehm XS, Ziehm XT, Ziehm XU, Ziehm XV, Ziehm XW, Ziehm XX, Ziehm XY, Ziehm XZ, Ziehm YA, Ziehm YB, Ziehm YC, Ziehm YD, Ziehm YE, Ziehm YF, Ziehm YG, Ziehm YH, Ziehm YI, Ziehm YJ, Ziehm YK, Ziehm YL, Ziehm YM, Ziehm YN, Ziehm YO, Ziehm YP, Ziehm YQ, Ziehm YR, Ziehm YS, Ziehm YT, Ziehm YU, Ziehm YV, Ziehm YW, Ziehm YX, Ziehm YY, Ziehm YZ, Ziehm ZA, Ziehm ZB, Ziehm ZC, Ziehm ZD, Ziehm ZE, Ziehm ZF, Ziehm ZG, Ziehm ZH, Ziehm ZI, Ziehm ZJ, Ziehm ZK, Ziehm ZL, Ziehm ZM, Ziehm ZN, Ziehm ZO, Ziehm ZP, Ziehm ZQ, Ziehm ZR, Ziehm ZS, Ziehm ZT, Ziehm ZU, Ziehm ZV, Ziehm ZW, Ziehm ZX, Ziehm ZY, Ziehm ZZ.

## SUPPORTING INFORMATION

Additional supporting information may be found online in the Supporting Information section at the end of the article.

**How to cite this article:** Kwiezinski C, Weller C, van Pinxteren D, Brüggemann M, Mertes S, Stratmann F, Herrmann H. Determination of highly polar compounds in atmospheric aerosol particles at ultra-trace levels using ion chromatography Orbitrap mass spectrometry. *J Sep Sci.* 2021;44:2343–2357.  
<https://doi.org/10.1002/jssc.202001048>